FERMILAB-PUB-14-008-A

Draft version December 11, 2013
Preprint typeset using LaTeX style emulateapj v. 5/2/11

ON THE MASS OF THE LOCAL GROUP

Roberto E. González[1,2,5], Andrey V. Kravtsov[1,2,3], and Nickolay Y. Gnedin[1,2,4]

Draft version December 11, 2013

ABSTRACT

We use recent proper motion measurements of the tangential velocity of M31, along with its radial velocity and distance, to derive the likelihood of the sum of halo masses of the Milky Way and M31. This is done using a sample halo pairs in the Bolshoi cosmological simulation of ΛCDM cosmology selected to match properties and environment of the Local Group. The resulting likelihood gives estimate of the sum of masses of $M_{\rm MW,200}+M_{\rm M31,200} = 2.40^{+1.95}_{-1.05}\times10^{12}\,M_\odot$ (90% confidence interval). This estimate is consistent with individual mass estimates for the Milky Way and M31 and is consistent, albeit somewhat on the low side, with the mass estimated using the timing argument. We show that although the timing argument is unbiased on average for all pairs, for pairs constrained to have radial and tangential velocities similar to that of the Local Group the argument overestimates the sum of masses by a factor of 1.6. Using similar technique we estimate the total dark matter mass enclosed within 1 Mpc from the Local Group barycenter to be $M_{\rm LG}(r<1\,{\rm Mpc}) = 4.2^{+3.4}_{-2.0}\times10^{12}\,M_\odot$ (90% confidence interval).

Subject headings: Galaxy: fundamental parameters, halo — galaxies: Local Group — dark matter

1. INTRODUCTION

Understanding the connection between dark matter (DM) halos and galaxies they host is a key question in galaxy formation theory. Theoretical models of hierarchical structure formation (White & Rees 1978; Fall & Efstathiou 1980; Blumenthal et al. 1984) envision dark matter halos to be the sites of galaxy formation and this framework is supported by a variety of observations (see, e.g., recent reviews by Frenk & White 2012; Courteau et al. 2013), such as galaxy rotation curves (Rubin & Ford 1970; Roberts & Rots 1973), X-ray halos (Forman et al. 1985; Buote & Canizares 1994; Buote et al. 2002; Humphrey et al. 2011; Bogdán et al. 2013, see Mathews & Brighenti 2003 for a review), satellite kinematics (Zaritsky et al. 1993, 1997; Zaritsky & White 1994; McKay et al. 2002; Prada et al. 2003; Conroy et al. 2007; Klypin & Prada 2009; More et al. 2011), and weak lensing measurements (e.g., Mandelbaum et al. 2006; van Uitert et al. 2011; Velander et al. 2013; Hudson et al. 2013).

The Local Group (LG hereafter) played an important role in establishing existence of extended massive halos around galaxies. Indeed, the first flat rotation curve was measured for M31 (Babcock 1939) and the mass estimate for the LG by Kahn & Woltjer (1959) was one of the very first compelling indications for existence of massive dark matter halos. The elegant argument in the latter study relied on the assumption that LG can be approximated by two point masses on a radial orbit on the first approach. Orbit integration backward in time, given the present day separation, velocity, and cosmological parameters, then constrains the mass of the system. This framework is now known as the timing argument (TA hereafter). Despite its simplicity and strong assumptions, the argument has withstood the test of time and new observations (Li & White 2008; van der Marel & Guhathakurta 2008; van der Marel et al. 2012). Nevertheless, the masses of both the Milky Way and M31 are both uncertain to a factor of two (e.g., Boylan-Kolchin et al. 2013, and references therein). Given the large uncertainties, the LG mass derived using the timing argument (Li & White 2008; van der Marel et al. 2012) is generally consistent with mass estimates derived using other methods (Klypin et al. 2002; Widrow & Dubinski 2005; Karachentsev et al. 2009; Watkins et al. 2010, and references therein), but is on the high side of the measurement range.

In this paper we present a different way to constrain the mass of the Local Group using approach similar to that used by Busha et al. (2011) to constrain the mass of the Milky Way. In this approach a set of observed properties of a system is used to estimate likelihood that a system in simulation is a counterpart of this system. Distribution of the likelihood as a function of halo mass can then be used to estimate the mass of observed system. In this study we select a population of the LG analogues from the Bolshoi cosmological simulation of ΛCDM cosmology (Klypin et al. 2011) and use observed properties of the MW and M31 to derive likelihood distribution for their combined mass.

We use several criteria to define the LG pair analogues in the cosmological simulation. In addition to distance and radial and tangential velocities, we also consider parameters characterizing environment, such as the distance to the nearest cluster, local large-scale density, and coldness of the local galaxy flow. The Local Group is known to reside in a region of rather low ("cold") radial velocity dispersion of galaxies, $\sigma_{\rm H} < 70{\rm km\,s^{-1}}$(Sandage & Tammann 1975; Governato et al. 1997; Karachentsev et al. 2003; Klypin et al. 2003; Aragon-Calvo et al. 2011, and references therein), as compared to velocity dispersion around MW-sized halos in the ΛCDM cosmology. This can be explained by the fact the LG is located in an average density environment (Klypin et al. 2003). We will explore in more detail this density and velocity dispersion relation, and use it to impose additional constrains to our LG analogues.

[1] Department of Astronomy & Astrophysics, The University of Chicago, Chicago, IL 60637 USA
[2] Kavli Institute for Cosmological Physics, The University of Chicago, Chicago, IL 60637 USA
[3] Enrico Fermi Institute, The University of Chicago, Chicago, IL 60637 USA
[4] Particle Astrophysics Center, Fermi National Accelerator Laboratory, Batavia, IL 60510 USA
[5] Instituto de Astrofísica, Pontificia Universidad Católica de Chile, Santiago, Chile regonzar@astro.puc.cl

Operated by Fermi Research Alliance, LLC under Contract No. De-AC02-07CH11359 with the United States Department of Energy.

The paper is organized as follows. In § 2 we describe the simulation and halo catalogs, while in § 3 we describe selection criteria for the LG analogues and different synthetic LG samples. We present our results for the likelihood distribution of the LG mass in § 4 and compare mass estimated using this method with previous estimates using the timing argument in § 5. We discuss our results and summarize conclusions in § 6. In this paper we use mass, M_{200}, defined as the mass within radius R_{200} enclosing the mean density of 200 times the critical density at the redshift of analysis. For the Milky Way-sized halos, M_{200} is related to the commonly used virial mass definition defined using cosmology and redshift dependent overdensity Bryan & Norman (1998) as $M_{\rm vir}/M_{200} \approx 1.2$.

2. SIMULATIONS AND HALO CATALOGS

To construct a sample of the Local Group analogues, we use halos from the Bolshoi simulation of ΛCDM cosmology: $\Omega_{\rm m} = 1 - \Omega_\Lambda = 0.27$, $H_0 = 70\,{\rm km/s/Mpc}$, $\sigma_8 = 0.82$, $n_s = 0.95$ (Klypin et al. 2011), compatible with the constraints from the WMAP satellite (Hinshaw et al. 2013). The simulation followed evolution of dark matter in a $250h^{-1}$Mpc box with spatial resolution of $\approx 1h^{-1}$ kpc and mass resolution of $m_{\rm p} = 1.35 \times 10^8$ M$_\odot$. Halos are identified with the BDM algorithm (Klypin & Holtzman 1997). The BDM algorithm is a spherical overdensity halo finding algorithm and is designed to identify both host halos and subhalos. In this study, however, we will only use the host halos.

The catalog of host halos is complete down to halos with maximum circular velocities of $\approx 50\,{\rm km\,s^{-1}}$, and we use only halos of larger mass to identify pairs of the MW-sized halos. To construct a sample of the MW-M31 pairs at $z \approx 0$, we use a series of simulation snapshots at $z < 0.1$ (i.e. in the last ≈ 1.3 Gyr before present) spaced by $\approx 150 - 250$ Myr, similarly to the strategy adopted in González et al. (2013). This is done because a particular configuration of MW and M31 is transient and would correspond to a relatively small number of systems at one snapshot. By using multiple snapshots we can increase the sample of systems in such configuration during a period of time in which secular cosmological evolution is small.

3. THE SAMPLE OF LOCAL GROUP ANALOGUES

The Local Group is dominated by the pair of the Milky Way and M31 and includes a number of smaller galaxies. Environment around the Local Group has density quite close to the average density of the universe (Klypin et al. 2003; Karachentsev 2005; Karachenstev 2012). In addition, the closest massive galaxy cluster, the Virgo Cluster, is ≈ 16.5 Mpc away (Mei et al. 2007). It is not clear to what extent the environment of the Local Group shapes its properties and dynamics. Therefore, we include environmental criteria in our set of selection criteria.

To identify the LG analogues, we first search for host halo pairs in which both members have masses in a wide range of masses from $M_{200c} = 5 \times 10^{10}$ M$_\odot$ to 5×10^{13} M$_\odot$ and are separated by $0.5 - 1.3$ Mpc. About a million host halos satisfy these criteria at the $z = 0$ snapshot. However, most of these pairs will be discarded in the next selection criteria, because they have low masses and are located in high density environment close to more massive structures.

Second, to select pairs in relative isolation and to avoid pairs in triplets or larger groups we define a quantitative isolation criterion using the force constraint $F_{i,{\rm com}} < \kappa F_{12}$, where $F_{i,{\rm com}}$ is the gravitational force between the pair and any neighbor halo i within a $5\,h^{-1}$Mpc radius of the pair center-of-mass, F_{12} is the force between the pair, and κ is a constant parameter. The isolation criterion becomes increasingly strict for decreasing values of κ. The Milky Way and M31 do not have massive neighbors within 5 Mpc, and should thus have $\kappa < 0.1$. The actual value of κ is, however, uncertain, and we use $\kappa = 0.25$ based on our previous tests reported in González et al. (2013).

The third selection criterion is intended to mimic the absence of massive clusters in the immediate vicinity of the Local Group. We require that halos in the LG sample have no neighbor halo with mass $M_{200} > 1.5{\times}10^{14}$ M$_\odot$ within 12 Mpc. The mass and distance limits are somewhat lower than the actual values for the Virgo Cluster (e.g., Fouqué et al. 2001; Nulsen & Bohringer 1995, and references therein) to allow for a larger number of systems.

We found 4177 pairs in the snapshot at $z = 0$ under these constraints, and for the full composite sample using 10 more snapshots at $z < 0.1$ we found 45844 pairs, which we use as the sample of LG analogues. We find that ≈ 80% of LG analogues in this sample are gravitationally bound under the two-body approximation. Note that the environment criteria are very restrictive: from the initial sample of pairs selected only by mass and separation, less than 1% satisfy the environment criteria.

4. MASS LIKELIHOOD

We compute the mass likelihood of the MW-M31 pairs using the sample of the LG analogues and method similar to that used by Busha et al. (2011) and González et al. (2013). Namely, for each of the LG analogues we compute the likelihood that the analogue matches a set of the actual LG properties and use the distribution of such likelihood values as a function of the sum of the two halo masses to estimate the range of the LG masses.

The specific properties we use in the calculation of likelihood are:

1. Galactocentric radial velocity, $V_{\rm RAD} = 109.3 \pm 4.4$ km s^{-1}, of M31 measured recently by Sohn et al. (2012).

2. Distance between M31 and MW, $\Delta r = 770 \pm 40$ kpc, adopted by van der Marel & Guhathakurta (2008) to span the range of recent measurements using different methods, tip of the red giant branch (Durrell et al. 2001; McConnachie et al. 2005), cepheids (Joshi et al. 2003; Karachentsev et al. 2004), and eclipsing binaries (Ribas et al. 2005).

3. The 1σ upper limit on the tangential component of M31 velocity relative to the Milky Way, $V_{\rm TAN} < 34.3$ km s^{-1}recently derived by Sohn et al. (2012).

4. We use the local environment constraint using the local velocity dispersion, $\sigma_{\rm H}$, and logarithm of the overdensity $\log(1+\delta)$ in a shell with inner radius of 1 Mpc, and outer radius of 5 Mpc from the pair center-of-mass. We use constraint of $\sigma_{\rm H} < 70$ km s^{-1} to reflect the range of observational estimates (see § 1). In the appendix we show that the velocity dispersion is correlated with overdensity, and that our fiducial choice of $\sigma_{\rm H} < 70$ km s^{-1} approximately corresponds to the upper limit on overdensity $\log(1+\delta) < 0.3$.

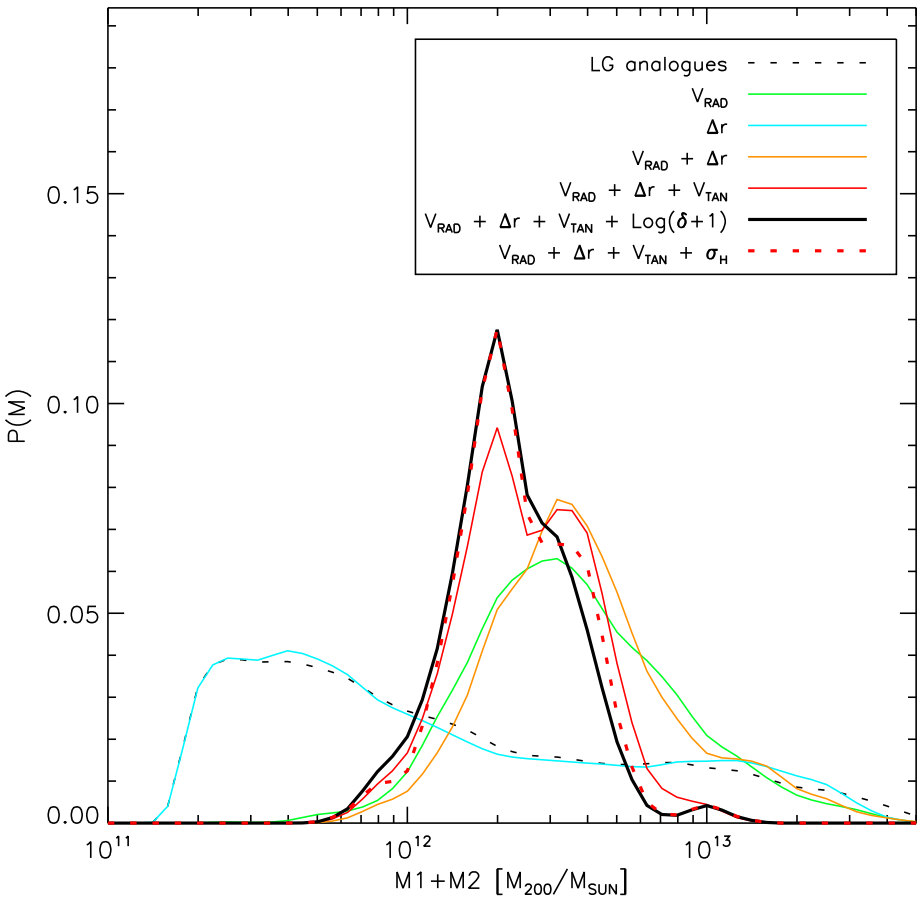

FIG. 1.— The likelihood distribution for the sum of M_{200} masses (mass within radius enclosing density equal to 200 times the critical density of the universe) of MW and M31 constructed using the LG halo pair analogues and using obsevational measurements of the relative separation and motion of MW and M31 with interval corresponding to 2σ of their measurement errors, as well as constraints on their environment (see legend). The median mass and corresponding 68% and 90% confidence intervals for each set of constraints are given in Table 1.

Our fiducial choice for the mass constraints presented in the paper is to use the range of observed values of constraint parameters with interval corresponding to $\pm 2\sigma$ of their observational errors. Namely, we use the following *rms* uncertainties: $\sigma_{V_{\rm RAD}} = 4.4$ km s^{-1} for radial velocity and $\sigma_{\Delta r} = 40$ kpc for separation. We do not have a complete information about the confidence interval for the tangential velocity and we use the estimate of the average tangential velocity of 17km s^{-1}and its 1σ upper limit of $V_{TAN} < 34.3$ km s^{-1}to extrapolate to 2σ upper limit of $V_{TAN} < 51.6$ km s^{-1}, and 3σ of $V_{TAN} < 68.6$ km s^{-1}. We have explored the effect of expanding our sample of pairs by increasing the error in radial velocity, separation and tangential velocity, and we found that the mass likelihood is stable, even when expanding the allowed constraint range corresponding to 3σ of their errors. A more detailed description of the tests for different constraints ranges can be found in the Appendix B.

Figure 1 shows the likelihood distribution for the sum of M_{200} masses of the two pair halos obtained for different constraint combinations. In table 1 we present the corresponding median values, with 68% and 90% confidence intervals and number of pairs in each sample. In addition, we present constraints on the mass within the radius of 1 Mpc from the pair barycenter in the last two rows of the table.

Figure 1 shows that the radial velocity of M31 provides the main constraint on the masses. Nevertheless, inclusion of the tangential velocity constraint eliminates the tail of objects at very high masses and shifts the peak of the likelihood to lower masses. This is because imposing constraint of low tangential velocity removes more massive pairs with higher orbital energies for a given fixed range of radial velocities.

The local density and velocity dispersion constraints do not affect the peak of the likelihood distribution but slightly narrow the width of the likelihood. Overall, we find that inclusion of the environment constraints in the likelihood calculations makes no significant difference: they shift the median and confidence intervals to masses $\approx 15\%$ lower.

We have explored the mass ratio distribution [6] for different samples following constraints from table 1 and found no effect of additional constraints on the mass ratio on the mass likelihood.

5. COMPARISON WITH THE PREVIOUS TIMING ARGUMENT MASS ESTIMATES

Li & White (2008, hereafter LW08), computed the bias

[6] Defined as the ratio between the halo mass of the smallest and largest pair member. The mass ratio of the MW/M31 pair is quite uncertain, but recent papers point toward a mass ratio close to unity, where M31 is somewhat more massive than the MW (Karachentsev et al. 2009; Reid et al. 2009; Baiesi Pillastrini 2009)

TABLE 1
MASS LIKELIHOOD OF MW+M31 PAIRS IN LG ANALOGUES

Constraints	$\log(M_{200}/M_\odot)$	68% conf. internval	90% conf. interval	N pairs
$V_{RAD} + \Delta r$	12.60	-0.10 +0.12	-0.31 +0.45	347
$V_{RAD} + \Delta r + V_{TAN}$	12.45	-0.12 +0.11	-0.25 +0.25	88
$V_{RAD} + \Delta r + V_{TAN} + \log(1+\delta)$	12.38	-0.07 +0.09	-0.25 +0.24	66
$V_{RAD} + \Delta r + V_{TAN} + \sigma_H$	12.39	-0.07 +0.13	-0.19 +0.27	64
$V_{RAD} + \Delta r + V_{TAN} + \log(1+\delta) + 1$ Mpc[a]	12.62	-0.11 +0.13	-0.28 +0.26	66
$V_{RAD} + \Delta r + V_{TAN} + \sigma_H + 1$Mpc	12.62	-0.11 -0.13	-0.28 +0.27	64

[a]The last two rows give constraints for the mass enclosed within 1 Mpc of the barycenter of the pair.

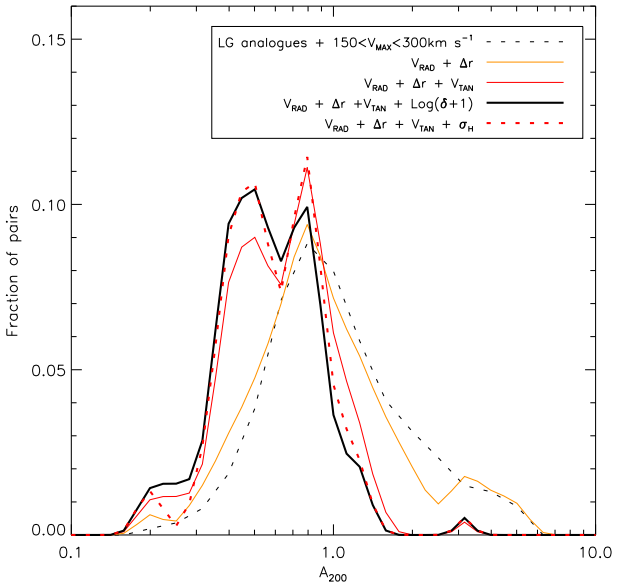

FIG. 2.— Ratio of the true pair mass and the TA mass estimate, A_{200}, for different combinations of constraints. In the case of radial velocity and separation constraints (orange), the median A_{200} is close to unity, but when tangential velocity constraint is included, the TA overestimates the true mass pushing the distribution to lower A_{200} values.

and error distribution of the TA estimator using LG-like systems in the Millenium Simulation. On average, they found good match between the true M_{200} masses of MW+M31 halos and the M_{TA} masses: $M_{TA} = 5.32 \pm 0.48 \times 10^{12}$ $M_\odot$, or $\log M_{TA}/M_\odot = [12.68, 12.76]$, which not even overlaps with our best 90% confidence interval from table 1(Third row). However, if we compute the TA mass using equations $(1-3)$ from their paper, but with updated radial velocity and separation values, we obtain a somewhat lower value of $M_{TA} = 4.14 \pm 0.60 \times 10^{12}$ $M_\odot$($\log M_{TA}/M_\odot = [12.55, 12.68]$) in good agreement with van der Marel et al. (2012). The decrease is due primarily to the lower radial velocity value compared to that used by LW08. Therefore, the TA mass range computed with updated velocity values is in good agreement with our likelihood estimate without taking into account tangential velocity and local environment (first two lines in Table 1). The somewhat lower estimate in our analysis is due then primarily to the tangential velocity and environment constraints, which shift the peak of the likelihood to smaller masses.

In figure 2, we show distribution of the ratio, $A_{200} = M_{200}(\mathrm{MW+M31})/M_{TA}$ (after LW08), of the true pair mass and the TA mass for different samples of LG analogues. The LG analogues sample with an additional cut of $150 < V_{max} < 300$ km s^{-1}(corresponding to the broad V_{max} selection of LW08), shows a distribution with median $A_{200} \approx 1.1$. If we use a narrower V_{max} range, the distribution also becomes narrower, in agreement with results of LW08 (see their Figures 1 and 2). For the radial velocity and distance constraint (orange) the median $A_{200} \approx 0.97$ but with a similar scatter.

Inclusion of the tangential velocity constraint in the selection of pairs (solid red), results in a narrow distribution with the median shifted to smaller value of $A_{200} \approx 0.75$, while inclusion of the additional local density or velocity dispersion constraint shifts the median to $A_{200} \approx 0.62$. This shows explicitly that the TA estimates works quite well for average halo pairs of separations and radial velocity. However, pairs with additional constraints on the tangential velocity and local density have systematically lower masses compared to the TA estimate. In other words, for such pairs the timing argument estimate overestimates mass by a factor of $\approx 1.3-1.6$. This explains the systematic difference between our fiducial constraint from the likelihood, $\log M_{200}(\mathrm{MW+M31}) \approx 12.38^{+0.09}_{-0.07}$ and the TA estimate $\log M_{200}(\mathrm{MW+M31}) \approx 12.62^{+0.06}_{-0.07}$. It is worth noting that it is quite surprising that the TA estimate works to within a factor of two, given how idealized the model underlying such estimate is. For example, the MW and M31 are approximated as point masses of constant mass on a purely radial orbit and surrounding mass distribution is neglected. At the same time, the mass evolution of MW and M31 is neglected as well. Finally the evolution of MW and M31 is envisioned within expanding background corresponding to the mean density of the universe and thus any dependence of expansion on the local overdensity is neglected. Given the simplicity of the model and a number of assumptions, it is quite remarkable that this model provides a reasonable ballpark estimate of mass. However, sensitivity to the tangential velocity and environment that we find shows that the accuracy of the TA estimate is ultimately limited.

Finally, we note that the mass estimate we derive from the likelihood is in reasonably good agreement with the recent abundance matching results (Kravtsov et al. 2013, see their Appendix), which for the stellar masses of 5×10^{10} $M_\odot$ and 9×10^{10} $M_\odot$ for the MW and M31, respectively, indicate average halo mass $M_{200}(\mathrm{MW+M31}) \approx 4.3 \times 10^{12}$ $M_\odot$ (or $\log_{10} M_{200}(\mathrm{MW+M31}) \approx 12.6$). This abundance matching result is based on the new measurement of the stellar mass function by Bernardi et al. (2013), which corrects significant photometric errors in the standard SDSS magnitudes.

The average scatter around this average value is thought to be $\approx$ 0.2 dex and although the scatter is large the agreement is encouraging, especially because previous abundance matching results by Moster et al. (2013) and Behroozi et al. (2013), based on older estimates of the stellar mass functions with SDSS photometry, indicated very large average mass of $M_{200}(\mathrm{MW+M31}) \approx 8-10\times10^{12}$ M$_\odot$ for the stellar masses of MW and M31. Reconciling low mass of the Local Group with abundance matching results would require assumption that MW and/or M31 are outliers from the average M_*-M_{200c} relation. However, better agreement with the new abundance matching M_*-M_{200} based on the stellar mass function of Bernardi et al. (2013) indicates that halo masses of the MW and M31 are consistent with the masses expected from the mean M_*-M_{200} relation.

6. DISCUSSION AND CONCLUSIONS

We define the LG analogues in the Bolshoi simulation of ΛCDM cosmology and estimate the MW-M31 pair mass likelihood in such systems. The analogues are selected as halo pairs using broad criteria. The sample is then used to estimate likelihood distribution of mass using several observed properties of the actual Local Group, namely separation, radial and tangential velocity, and density of the local environment. To characterize the latter, we compute the DM overdensity and particle velocity dispersion, $\sigma_{\rm H}$, within 5 Mpc from halo pair center of mass. We found a tight correlation between local overdensity and velocity dispersion estimated within 5 Mpc (see Appendix), so that constraint on overdensity is approximately equivalent to the constraint on the velocity dispersion. To set the environment constraint we require $\sigma_{\rm H} < 70$ km s^{-1} (or $\log(\delta+1) < 0.3$) based on the observational values of this dispersion reported in the literature. At a given snapshot around $z=0$, about 2% of the MW-sized ($M_{200}\sim10^{12}$ M$_\odot$) halos satisfy our broad LG analogue criteria, and less than 5% of these two per cent satisfy the additional orbital and environment constraints.

We have shown that the main parameter controlling the MW-M31 mass likelihood is radial velocity. However, we also show that the likelihood is sensitive to the constraints on tangential velocity. In particular, we find that mass likelihood peak shifts to lower masses when constraint on the tangential velocity is included. This is because this constraint eliminates massive pairs with a given radial velocity range. Note that there is no such sensitivity to the tangential velocity in the timing argument estimate because neither the tangential velocity nor environment are taken into account in such estimate. Indeed, the mass constrain we derive from the likelihood is in good agreement with the mass estimate from the timing argument when only radial velocity and separation are used as constraints: $M_{\rm TA} = 4.14\pm0.60\times10^{12}$ M$_\odot$, in agreement with van der Marel et al. (2012) results, but somewhat lower than LW08 due to lower updated value of the radial velocity used in our estimate. However, when we add tangential velocity and environment constraints the median of the likelihood shifts to lower masses by a factor of ≈ 1.6. We show explicitly that for pairs with low tangential velocities and low local overdensity and velocity dispersion, the timing argument overestimates true masses of the pair by an average factor of ≈ 1.6, thereby explaining the lower values derived from the likelihood method. These values are summarized in Table 1: our fiducial mass estimate obtained including the local density constraint is $M_{\rm MW,200c}+M_{\rm M31,200c} = 2.40^{+0.55}_{-0.36}\times10^{12}M_\odot$ (68% confidence interval). For this sample we have also computed the DM mass enclosed within 1 Mpc from the pair center of mass: $M_{\rm LG}(r<1\mathrm{Mpc}) = 4.17^{+1.45}_{-0.93}\times10^{12}M_\odot$ (68% confidence interval).

Overall, the values we deduce for the sum of the Milky Way and M31 halo masses are consistent with existing constraints on the individual halo masses of the Milky Way (see, e.g., Boylan-Kolchin et al. 2012, 2013, and references therein) and M31 (Widrow & Dubinski 2005). Given that the estimates of halo mass using satellite velocity (e.g., Boylan-Kolchin et al. 2013) can give robust lower limits to individual halo masses, combination of the estimates of the combined LG mass and individual masses should help to narrow down the range of possible masses for our Galaxy and for our closest neighbor, M31.

We would like to thank Anatoly Klypin for making the Bolshoi simulation and the BDM halo catalogs publicly available. This work was supported by NSF via grant OCI-0904482. AK was in addition supported in part by NSF grants AST-0807444 and by the Kavli Institute for Cosmological Physics at the University of Chicago through the NSF grant PHY-0551142 and PHY- 1125897 and an endowment from the Kavli Foundation. We have made extensive use of the NASA Astrophysics Data System and `arXiv.org` preprint server.

APPENDIX

A. COLD LOCAL HUBBLE FLOW

In order to characterize the local environment of the LG we use the velocity dispersion $\sigma_{\rm H}$ of nearby galaxies. It is known that this velocity dispersion is rather low within a few Mpc from the Local Group, compared to the velocity dispersion expected for MW-sized halos in simulations (e.g., Governato et al. 1997). This "coldness" of the local Hubble flow was noted for quite some time in studies measuring the Hubble constant with local galaxies (de Vaucouleurs 1958; Sandage & Tammann 1975). The values of velocity dispersion were consistently found to be around $\sigma_{\rm H}\sim60$ km s^{-1} up to 8 Mpc (Sandage & Tammann 1975; Giraud 1986; Ekholm et al. 2001; Karachentsev et al. 2009, 2003; Macciò et al. 2005; Tikhonov & Klypin 2009; Klypin et al. 2003; Aragon-Calvo et al. 2011). However, the local velocity dispersion increases with the maximum radius adopted to measure it (Sandage & Tammann 1975; Macciò et al. 2005; Tikhonov & Klypin 2009), and thus the specific value of the velocity dispersion used for constraints should correspond to the radius used in observations.

Furthermore, the methodology to compute the local velocity dispersion must also be taken into account when comparing different results; i.e., Karachentsev et al. (2003) found $\sigma_{\rm H} = 85$ km s^{-1} within 5 Mpc, but the estimate drops to $\sigma_{\rm H} = 41$ km s^{-1} when members of the M81 and Cen A groups are removed. We adopt the conservative value of $\sigma_{\rm H} < 70$ km s^{-1} as a constraint for the mass likelihood computation. The coldness of the local flow can be attributed to the relative isolation of the LG, and the relatively low density of the LG environment (Klypin et al. 2003; Martinez-Vaquero et al. 2009).

Macciò et al. (2005) found correlation between $\sigma_{\rm H}$ and local density in ΛCDM numerical simulations and pointed out that observational velocity dispersion measurements around the Local Group imply overdensity of $-0.1<\delta\rho/\rho<0.6$ on the scale of 7 Mpc. We explore the $\sigma_{\rm H}$–overdensity relation

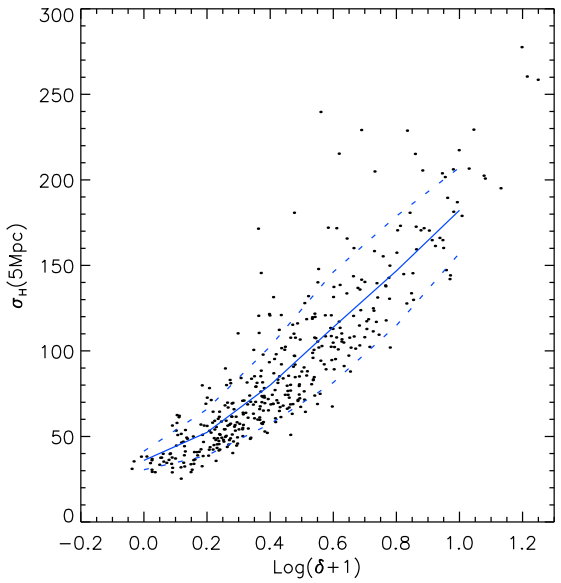

FIG. 3.— The local overdensity and velocity dispersion relation for the MW-sized halos in the Local Group analogues sample. Blue lines show the mean and standard deviation of the distribution. Density and velocity dispersion are computed using DM particles within a shell ranging from 1 to 5 Mpc.

for our sample of LG analogues, estimating $\sigma_{\rm H}$ using halos and dark matter particles with respect to the pair center of mass. For the former we compute the radial peculiar velocity of host halos with maximum circular velocities of $V_{\rm max} > 50$ km s^{-1}. For the latter estimate we use DM particles outside $3 \times R_{200}$ from any halos with $V_{\rm max} > 50$.

Halos should be closer to galaxy tracers used in observations, but for some pairs the number of halos is too low for an adequate $\sigma_{\rm H}$ computation. On the other hand, using particles gives a robust $\sigma_{\rm H}$ computation in all cases, but makes comparison with observations more ambiguous. There is an overall scatter of $\sim$ 40 km s^{-1} between the two estimates of $\sigma_{\rm H}$, which decreases to $\approx$ 25 km s^{-1}, for velocity dispersions lower than 100 km s^{-1}. In both cases, $\sigma_{\rm H}$ is computed in shells with the radius ranging within 1−5 Mpc. The lower limit is set because the Hubble flow is observed only at $R_0 \gtrsim 1$ Mpc (e.g., Karachenstev 2012). This can be used to put an upper limit to the mass of the LG (Ekholm et al. 2001; Karachentsev et al. 2002, 2009).

In figure 3, we show the $\sigma_{\rm H}$–overdensity relation estimated around the LG analogues, in which each pair member is in the mass range of $0.8 - 2.9 \times 10^{12}$ M$_\odot$ chosen to follow sample definition from González et al. (2013). We see a fairly tight relation at low σ_H values in agreement with Macciò et al. (2005) with 20%, 43%, and 65% of the LG analogues having σ_H lower than 50, 70, and 100 km s^{-1}, which corresponds to the average overdensities of $\log(1+\delta) = 0.156$, 0.237, and 0.303, respectively. For the mass likelihood estimate, we use the constraint $\log(1+\delta) < 0.3$ corresponding to systems with $\sigma_{\rm H} < 70$ km s^{-1} on average.

B. SENSITIVITY OF THE MASS LIKELIHOOD DISTRIBUTION TO CONSTRAINT CHOICES

The pair separation, radial and tangential velocity are the main orbital constraints used for the mass likelihood computation. They are very restrictive due their small associated errors resulting in small number of halo pairs. The samples can be increased if we relax these constraints and assume instead that the errors for a particular parameter are two or three times larger than the actual errors. In this section we investigate the effect of such choices used as a constraint in calculation of the likelihood distribution. Larger adopted error allows to increase the size of the halo samples and decrease the associated Poisson errors. However, it means that we allow for inclusion of objects less consistent with observational constraints. The actual choice of the error is a trade-off between these two considerations.

TABLE 2
MASS LIKELIHOOD DEPENDENCE ON $V_{\rm RAD}$ CONSTRAINT AMPLITUDE

$\sigma(V_{\rm RAD})/(4.4$ km s$^{-1})$	$\log(M_{200}/{\rm M}_\odot)$	90% c. i.	68% c. i.
1.0	12.38	-0.13 +0.29	-0.05 +0.19
1.5	12.35	-0.29 +0.32	-0.10 +0.17
2.0	12.51	-0.31 +0.27	-0.19 +0.11
2.5	12.48	-0.28 +0.22	-0.17 +0.12
3.0	12.51	-0.31 +0.19	-0.17 +0.09
3.5	12.51	-0.32 +0.27	-0.17 +0.09
4.0	12.51	-0.40 +0.28	-0.17 +0.11

TABLE 3
MASS LIKELIHOOD DEPENDENCE ON Δr CONSTRAINT AMPLITUDE

$\sigma(\Delta r)/(40$ kpc)	$\log(M_{200}/{\rm M}_\odot)$	90% c. i.	68% c. i.
2.0	12.36	-0.12 +0.31	-0.04 +0.17
3.0	12.37	-0.24 +0.30	-0.07 +0.13

The 1σ error for distance and radial velocity are $\sigma(\Delta r) = 40$ kpc, and $\sigma(V_{\rm RAD}) = 4.4$ km s^{-1}. The mean value of the tangential velocity is 17 km s^{-1}with 1σ upper limit of $V_{\rm TAN} <$ 34.3 km s^{-1}, which we extrapolate to 2σ and 3σ upper limits of $V_{\rm TAN} <$ 51.6 km s^{-1} and $V_{\rm TAN} <$ 68.6 km s^{-1}, respectively. We repeat our likelihood calculations using errors of constraint parameter inflated by a factor of three for each constraint separately and for all combined constraints. Here we do not include environment constraint, given that we found that their effect is relatively small.

In the first test, we keep the errors for distance and tangential velocity fixed to their respective 1σ values, while we change the error of $\sigma(V_{\rm RAD})$. Results are listed in Table 2, which shows that the median mass value increases when the error of radial velocity is increased from ±4.4 km s^{-1}to 8.8 km s^{-1}, but is not sensitive to further increase due to combined constraints to all of the other parameters. The 68% and 90% confidence intervals also increase somewhat with increasing error. The number of pairs increase from 12 to 60 for 1σ to 4σ values.

In the second test, we have kept the errors of radial and tangential velocity fixed at 1σ, but increased error of distance, $\sigma(\Delta r)$ (Table 3). The median mass and 68% confidence interval are not sensitive to increases in the distance errors, while 90% confidence interval increases somewhat. At 3σ the number of pairs increases to 40.

TABLE 4
MASS LIKELIHOOD DEPENDENCE ON V_{TAN} CONSTRAINT AMPLITUDE

$V_{TAN}/(\mathrm{km\,s^{-1}})$	$\log(M_{200}/\mathrm{M_\odot})$	90% c. i.	68% c. i.
51.6	12.38	-0.14 +0.39	-0.07 +0.20
68.6	12.54	-0.29 +0.23	-0.19 +0.05

TABLE 5
MASS LIKELIHOOD DEPENDENCE ON INCREASING ALL CONSTRAINTS AMPLITUDES

$\sigma(\mathrm{test})/\sigma$	$\log(M_{200}/\mathrm{M_\odot})$	90% c. i.	68% c. i.
1.0	12.38	-0.13 +0.29	-0.05 +0.19
2.0	12.45	-0.25 +0.25	-0.12 +0.11
3.0	12.44	-0.32 +0.27	-0.13 +0.11

In the third test we have kept the radial velocity and separation errors fixed at 1σ, while varying the adopted error of $\sigma(V_{TAN})$ (Table 4). Increase of the tangential velocity constraint to 51.6 $\mathrm{km\,s^{-1}}(2\sigma)$ does not change the median, while increase to 68.6 $\mathrm{km\,s^{-1}}(3\sigma)$ leads to increase of the median mass value and the confidence intervals. The number of pairs increases to 20 and 31 for 2σ and 3σ respectively.

Finally, when we vary errors of all of the constraining parameters simultaneously (Table 5), the median mass value increases by less than 1σ when errors are inflated by a factor of two. The main effect on the confidence intervals is to increase the range of mass values smaller than the median, while the upper error bar does not change and even decreases slightly.

These tests indicate the our results for the mass likelihood do not depend sensitively to our fiducial choice to inflate observed errors by a factor of two. In fact, if anything, the derived mass constraint for the actual observational errors is slightly smaller with smaller error bars. In this case, however, the sample contains only 12 pairs. We therefore think that our fiducial choice is more conservative.

REFERENCES

Aragon-Calvo, M. A., Silk, J., & Szalay, A. S. 2011, MNRAS, 415, L16
Babcock, H. W. 1939, Lick Observatory Bulletin, 19, 41
Baiesi Pillastrini, G. C. 2009, MNRAS, 397, 1990
Behroozi, P. S., Wechsler, R. H., & Conroy, C. 2013, ApJ, 770, 57
Bernardi, M., Meert, A., Sheth, R. K., Vikram, V., Huertas-Company, M., Mei, S., & Shankar, F. 2013, MNRAS submitted (arxiv/1304.7778)
Blumenthal, G. R., Faber, S. M., Primack, J. R., & Rees, M. J. 1984, Nature, 311, 517
Bogdán, Á., et al. 2013, ApJ, 772, 97
Boylan-Kolchin, M., Bullock, J. S., & Kaplinghat, M. 2012, MNRAS, 422, 1203
Boylan-Kolchin, M., Bullock, J. S., Sohn, S. T., Besla, G., & van der Marel, R. P. 2013, ApJ, 768, 140
Bryan, G. L., & Norman, M. L. 1998, ApJ, 495, 80
Buote, D. A., & Canizares, C. R. 1994, ApJ, 427, 86
Buote, D. A., Jeltema, T. E., Canizares, C. R., & Garmire, G. P. 2002, ApJ, 577, 183
Busha, M. T., Marshall, P. J., Wechsler, R. H., Klypin, A., & Primack, J. 2011, ApJ, 743, 40
Conroy, C., et al. 2007, ApJ, 654, 153
Courteau, S., et al. 2013, arxiv/1309.3276
de Vaucouleurs, G. 1958, AJ, 63, 253
Durrell, P. R., Harris, W. E., & Pritchet, C. J. 2001, AJ, 121, 2557
Ekholm, T., Baryshev, Y., Teerikorpi, P., Hanski, M. O., & Paturel, G. 2001, A&A, 368, L17
Fall, S. M., & Efstathiou, G. 1980, MNRAS, 193, 189
Forman, W., Jones, C., & Tucker, W. 1985, ApJ, 293, 102
Fouqué, P., Solanes, J. M., Sanchis, T., & Balkowski, C. 2001, A&A, 375, 770
Frenk, C. S., & White, S. D. M. 2012, Annalen der Physik, 524, 507
Giraud, E. 1986, A&A, 170, 1
González, R. E., Kravtsov, A. V., & Gnedin, N. Y. 2013, ApJ, 770, 96
Governato, F., Moore, B., Cen, R., Stadel, J., Lake, G., & Quinn, T. 1997, New Astronomy, 2, 91
Hinshaw, G., et al. 2013, ApJS, 208, 19
Hudson, M. J., et al. 2013, MNRAS submitted (arXiv/1310.6784)
Humphrey, P. J., Buote, D. A., Canizares, C. R., Fabian, A. C., & Miller, J. M. 2011, ApJ, 729, 53
Joshi, Y. C., Pandey, A. K., Narasimha, D., Sagar, R., & Giraud-Héraud, Y. 2003, A&A, 402, 113
Kahn, F. D., & Woltjer, L. 1959, ApJ, 130, 705
Karachenstev, I. D. 2012, http://arxiv.org/abs/1204.3377
Karachentsev, I. D. 2005, AJ, 129, 178
Karachentsev, I. D., Karachentseva, V. E., Huchtmeier, W. K., & Makarov, D. I. 2004, AJ, 127, 2031
Karachentsev, I. D., Kashibadze, O. G., Makarov, D. I., & Tully, R. B. 2009, MNRAS, 393, 1265
Karachentsev, I. D., et al. 2002, A&A, 389, 812
—. 2003, A&A, 398, 479
Klypin, A., Hoffman, Y., Kravtsov, A. V., & Gottlöber, S. 2003, ApJ, 596, 19
Klypin, A., & Holtzman, J. 1997, ArXiv Astrophysics e-prints
Klypin, A., & Prada, F. 2009, ApJ, 690, 1488
Klypin, A., Zhao, H., & Somerville, R. S. 2002, ApJ, 573, 597
Klypin, A. A., Trujillo-Gomez, S., & Primack, J. 2011, ApJ, 740, 102
Kravtsov, A., Vikhlinin, A., & Mescheryakov, A. 2013, ApJ submitted
Li, Y.-S., & White, S. D. M. 2008, MNRAS, 384, 1459
Macciò, A. V., Governato, F., & Horellou, C. 2005, MNRAS, 359, 941
Mandelbaum, R., Seljak, U., Kauffmann, G., Hirata, C. M., & Brinkmann, J. 2006, MNRAS, 368, 715
Martinez-Vaquero, L. A., Yepes, G., Hoffman, Y., Gottlöber, S., & Sivan, M. 2009, MNRAS, 397, 2070
Mathews, W. G., & Brighenti, F. 2003, ARA&A, 41, 191
McConnachie, A. W., Irwin, M. J., Ferguson, A. M. N., Ibata, R. A., Lewis, G. F., & Tanvir, N. 2005, MNRAS, 356, 979
McKay, T. A., et al. 2002, ApJ, 571, L85
Mei, S., et al. 2007, ApJ, 655, 144
More, S., van den Bosch, F. C., Cacciato, M., Skibba, R., Mo, H. J., & Yang, X. 2011, MNRAS, 410, 210
Moster, B. P., Naab, T., & White, S. D. M. 2013, MNRAS, 428, 3121
Nulsen, P. E. J., & Bohringer, H. 1995, MNRAS, 274, 1093
Prada, F., et al. 2003, ApJ, 598, 260
Reid, M. J., et al. 2009, ApJ, 700, 137
Ribas, I., Jordi, C., Vilardell, F., Fitzpatrick, E. L., Hilditch, R. W., & Guinan, E. F. 2005, ApJ, 635, L37
Roberts, M. S., & Rots, A. H. 1973, A&A, 26, 483
Rubin, V. C., & Ford, Jr., W. K. 1970, ApJ, 159, 379
Sandage, A., & Tammann, G. A. 1975, ApJ, 196, 313
Sohn, S. T., Anderson, J., & van der Marel, R. P. 2012, ApJ, 753, 7
Tikhonov, A. V., & Klypin, A. 2009, MNRAS, 395, 1915
van der Marel, R. P., Fardal, M., Besla, G., Beaton, R. L., Sohn, S. T., Anderson, J., Brown, T., & Guhathakurta, P. 2012, ApJ, 753, 8
van der Marel, R. P., & Guhathakurta, P. 2008, ApJ, 678, 187
van Uitert, E., Hoekstra, H., Velander, M., Gilbank, D. G., Gladders, M. D., & Yee, H. K. C. 2011, A&A, 534, A14
Velander, M., et al. 2013, MNRAS in press (arxiv/1304.4265)
Watkins, L. L., Evans, N. W., & An, J. H. 2010, MNRAS, 406, 264
White, S. D. M., & Rees, M. J. 1978, MNRAS, 183, 341
Widrow, L. M., & Dubinski, J. 2005, ApJ, 631, 838
Zaritsky, D., Smith, R., Frenk, C., & White, S. D. M. 1993, ApJ, 405, 464
—. 1997, ApJ, 478, 39

Zaritsky, D., & White, S. D. M. 1994, ApJ, 435, 599